Diffraction of Electromagnetic Plane Wave by a Rectangular Plate and a Rectangular Hole in the Conducting Plate

Kohei Hongo and Hirohide Serizawa

***Abstract*— The problems of diffraction of an electromagnetic plane wave by a perfectly conducting rectangular plate and its complementary problem—diffraction by a rectangular hole in an infinite conducting plate—are rigorously solved using the method of the Kobayashi potential. The mathematical formulation involves dual integral equations derived from the potential integrals and boundary condition on the plane where a plate or hole is located. The weighting functions in the potential integrals are determined by applying the properties of the Weber–Schafheitlin's integrals and the solution is obtained in the form of a matrix equation. Illustrative computations are given for the far diffracted field pattern and the current densities induced on the plate. The results of the patterns are compared with the results obtained from physical optics (PO) and the physical theory of diffraction (PTD). The agreement is fairly good, particularly with the PTD solutions.**

***Index Terms*—Apertures, electromagnetic diffraction, plates.**

I. Introduction

THE problem of electromagnetic diffraction by an aperture in a perfectly conducting plane of infinite extent has received considerable attention [1]–[4]. The solution can be applied to the complementary problem; that is, diffraction by a perfectly conducting plate using the Babinet's principle when the plate is negligibly thin. Most researchers have used an integral equation for unknown equivalent surface current density on the aperture or plate. This integral equation is reduced to a matrix equation via the method of moments (MoM).

In this paper, rigorous solutions to the problem of a plane wave scattering by a rectangular conducting plate and its complementary problem (diffraction by a rectangular hole in a perfectly conducting plane) are derived using the method of the Kobayashi potential (KP method) [5], [6]. This method has been applied to various kinds of problems such as the potential problems of electrified circular disks [7], [8], the diffraction of acoustic waves by a circular disk (or disks) [9], and the diffraction of acoustic plane wave by a rectangular plate [10], [11]. The KP method has also been used for diffraction of electromagnetic waves by a thick slit [12], a flanged parallel-plate waveguide [13], an N-slit array [14], a circular disk [15], [16], etc.

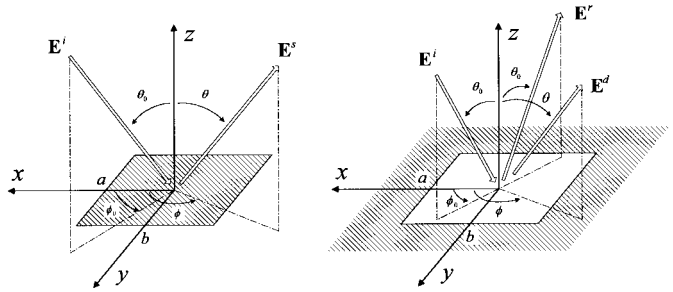

Fig. 1. Geometry of problem. (a) Perfectly conducting rectangular plate. (b) Rectangular hole in perfectly conducting plate (plate and hole are $2a \times 2b$).

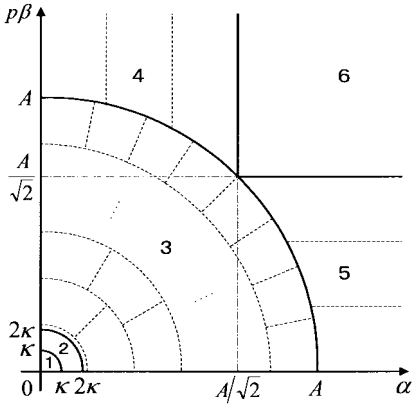

Fig. 2. Integration region subdivided into many subregions. Gauss Legendre quadrature applied in regions 1–3 and asymptotic approximation of Bessel functions applied to integrand in regions 4–6.

The KP method resembles the MoM in its spectrum domain, but the formulation is different. The MoM is based on an integral equation, whereas the KP method starts from dual integral equations. The MoM in a space domain has been used mostly in the diffraction problems of electromagnetic waves. We can cite the following advantages of the KP method over the current numerical techniques (mainly over MoM).

1) In contrast to the MoM in a space domain, the KP method does not involve singularities of the Green's functions, so we can obtain very accurate results.
2) Since each function involved in the integrand of the potential functions satisfies a part of the required boundary

Manuscript received December 31, 1997; revised October 29, 1998.

K. Hongo is with the Department of Information Science, Toho University, Funabashi, 274-0072 Japan.

H. Serizawa is with the Department of Control and Computer Engineering, Numazu, College of Technology, Numazu, 410-8501 Japan.

Publisher Item Identifier S 0018-926X(99)05812-3.

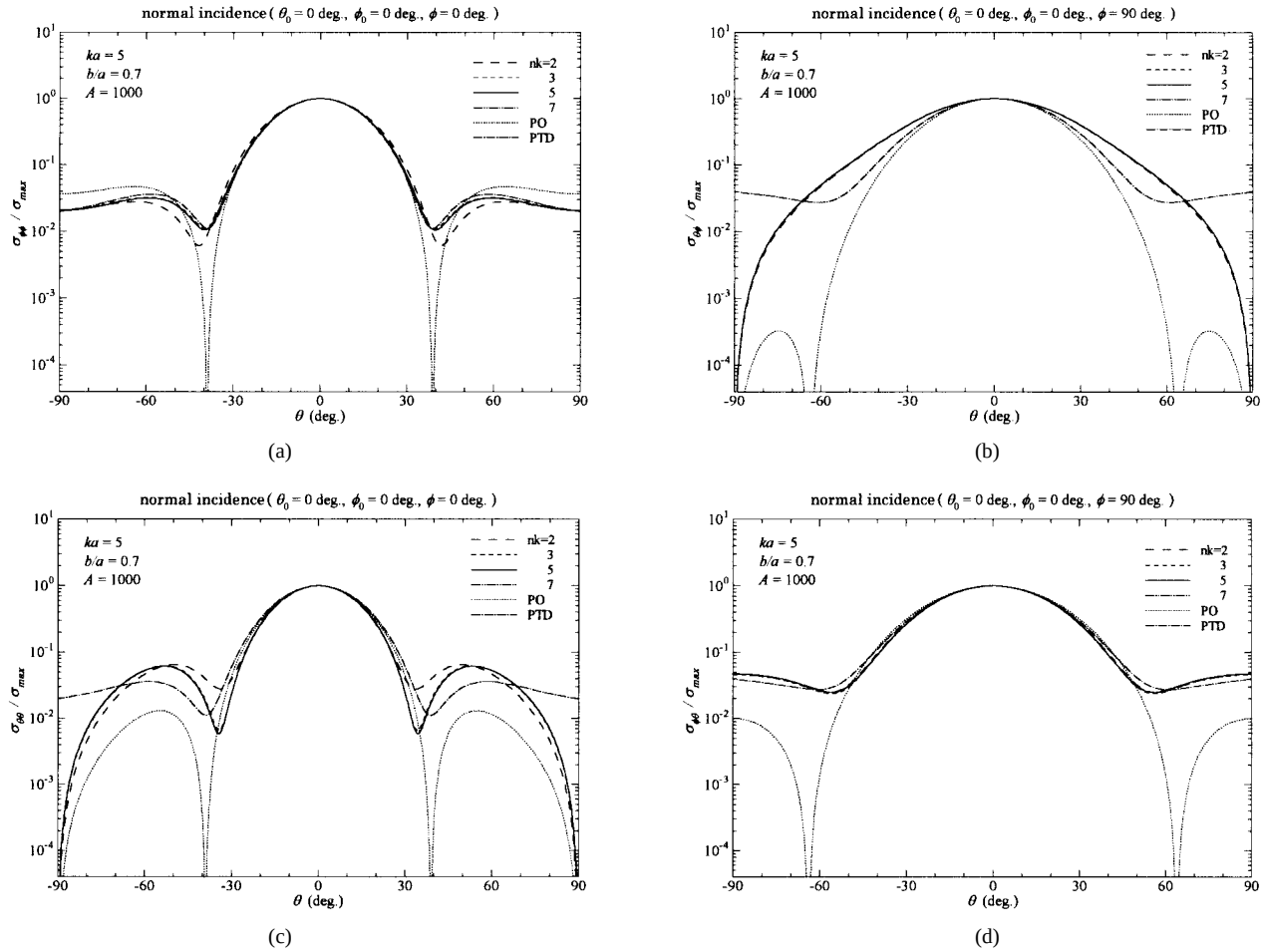

Fig. 3. Far-field pattern diffracted by a perfectly conducting rectangular plate for normal incidence $(\theta_0 = 0^\circ, \phi_0 = 0^\circ)$. Plate is $\kappa = ka = 5$ for (a)–(d). First subscript of σ denotes diffracted field component and second subscript denotes incident wave polarization.

conditions, the convergence is very rapid. In this respect, the present method may be regarded as eigenfunction expansion of the geometries. The required matrix size in the present case is roughly $2(ka)^2 \times 2(ka)^2$, where a is the linear dimension of the plate and k is the wave number.

3) As in two-dimensional (2-D) problems, the KP method may be applied to more complex problems with related configurations. These problems may be formulated in a manner similar to the eigenfunction expansions in cylindrical and spherical geometries.
4) For 2-D problems, the solution to a two-slit diffraction can be used to predict the coupling between the slits asymptotically [17]. This is also expected in three-dimensional (3-D) problems.

The disadvantage is that the tractable geometries of this method are limited to special shapes like rectangular and circular plates and their related geometries. A similar situation is seen for other conventional eigenfunction expansions.

The solution begins by introducing the Fourier sine and cosine transforms of the tangential components of the vector potentials. From the requirement of the boundary conditions on the plane exterior to the plate or hole, we obtain the dual integral equations for the transformed functions (or weighting functions). The equations are solved by using the properties of the Weber–Schafheitlin discontinuous integrals. At this step, we can incorporate the required edge condition into the solution. The results include two kinds of arbitrary discrete parameters, so that the general solution is obtained by superposing these results. By imposing the remaining boundary conditions on the plate or on the aperture, we have a matrix equation for the expansion coefficients. Matrix elements are given by double infinte integrals as in the method of moments in the spectral domain. We apply an algorithm, which is effective at computing these integrals [11], to compute these matrix elements. We present numerical results for the far diffracted pattern and current distributions, and compare the results of the far-field patterns with the corresponding PO and PTD solutions. Their agreement is fairly good, but the PTD results are closer to results presented here.

II. Statement of the Problem

The geometry of the problem and the associated coordinates are described in Fig. 1, where the dimension of the plate and hole is $2a \times 2b$. Two kinds of incident plane waves are considered, which are expressed by

$$\mathbf{E}^i = (E_2\mathbf{i}_\theta + E_1\mathbf{i}_\phi)\exp[jk\Phi^i(\mathbf{r})] \tag{1a}$$

$$\mathbf{H}^i = Y_0(-E_2\mathbf{i}_\phi + E_1\mathbf{i}_\theta)\exp[jk\Phi^i(\mathbf{r})] \tag{1b}$$

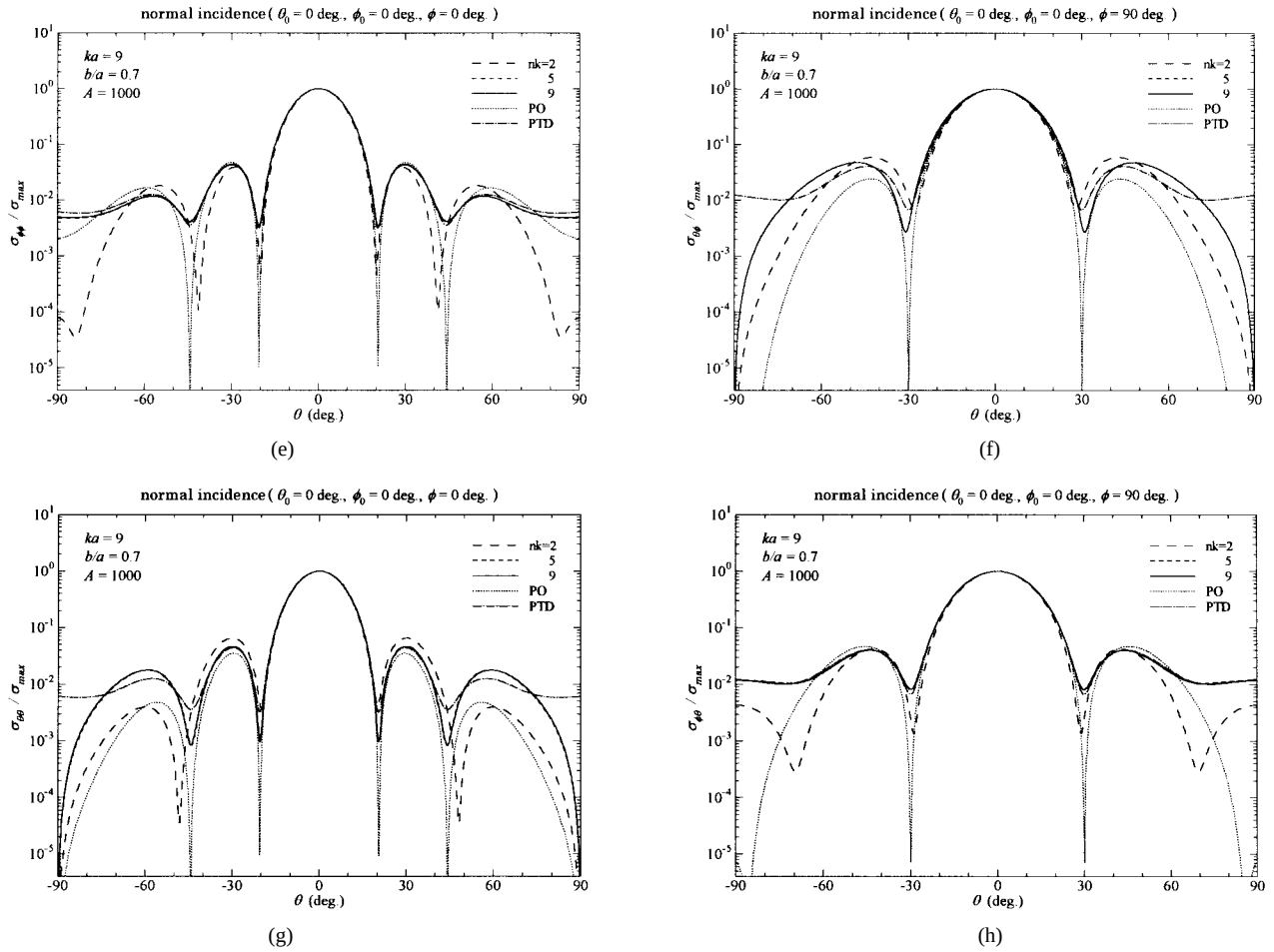

Fig. 3. (*Continued.*) Far-field pattern diffracted by a perfectly conducting rectangular plate for normal incidence ($\theta_0 = 0^\circ, \phi_0 = 0^\circ$). Plate is $\kappa = 9$ for (e)–(h). First subscript of σ denotes diffracted field component and second subscript denotes incident wave polarization.

where

$$\mathbf{i}_\theta = \cos\theta_0\cos\phi_0\mathbf{i}_x + \cos\theta_0\sin\phi_0\mathbf{i}_y - \sin\theta_0\mathbf{i}_z$$
$$\mathbf{i}_\phi = -\sin\phi_0\mathbf{i}_x + \cos\phi_0\mathbf{i}_y \quad (1c)$$
$$\Phi^i(\mathbf{r}) = x\sin\theta_0\cos\phi_0 + y\sin\theta_0\sin\phi_0 + z\cos\theta_0. \quad (1d)$$

We refer to parallel polarization in which the electric field of the incident wave is proportional to E_2, while the wave proportional to E_1 is called perpendicular polarization. In the above equations, (θ_0, ϕ_0) are angles of incidence and $Y_0 = \sqrt{\frac{\epsilon}{\mu}}$ is an intrinsic admittance of free-space. When the plane $z = 0$ is occupied by an infinite conducting plate, a reflected wave is produced and it is given by

$$\mathbf{E}^r = [(\sin\phi_0\mathbf{i}_x - \cos\phi_0\mathbf{i}_y)E_1 - (\cos\theta_0\cos\phi_0\mathbf{i}_x + \cos\theta_0\sin\phi_0\mathbf{i}_y + \sin\theta_0\mathbf{i}_z)E_2]\exp[jk\Phi^r] \quad (2a)$$
$$\mathbf{H}^r = Y_0[(\cos\theta_0\cos\phi_0\mathbf{i}_x + \cos\theta_0\sin\phi_0\mathbf{i}_y + \sin\theta_0\mathbf{i}_z)E_1 + (\sin\phi_0\mathbf{i}_x - \cos\phi_0\mathbf{i}_y)E_2]\exp[jk\Phi^r] \quad (2b)$$

where

$$\Phi^r(\mathbf{r}) = x\sin\theta_0\cos\phi_0 + y\sin\theta_0\sin\phi_0 - z\cos\theta_0 \quad (2c)$$

is the phase of the reflected wave.

III. Analytical Development

A. Solution of the Diffracted Field

We use the tangential components of the magnetic vector potential A_x^d and A_y^d to derive the field diffracted by a perfectly conducting plate. From the duality of the electromagnetic fields, the complementary problem may be solved using the electric vector potentials F_x^d and F_y^d. With the Fourier sine and cosine transforms, these vector potentials are given in a form

$$\begin{pmatrix} A_x^d \\ F_x^d \end{pmatrix} = \begin{pmatrix} \mu Y_0 \\ \mp\epsilon \end{pmatrix}\int_0^\infty\int_0^\infty [f_{cc}(\alpha,\beta)\cos\alpha\xi\cos\beta\eta + f_{cs}(\alpha,\beta)\cos\alpha\xi\sin\beta\eta + f_{sc}(\alpha,\beta)\sin\alpha\xi\cos\beta\eta + f_{ss}(\alpha,\beta)\sin\alpha\xi\sin\beta\eta]\exp[\mp\zeta(\alpha,\beta)z_a]\,d\alpha\,d\beta \quad z \gtrless 0 \quad (3a)$$

$$\begin{pmatrix} A_y^d \\ F_y^d \end{pmatrix} = \begin{pmatrix} \mu Y_0 \\ \mp\epsilon \end{pmatrix}\int_0^\infty\int_0^\infty [g_{cc}(\alpha,\beta)\cos\alpha\xi\cos\beta\eta + g_{cs}(\alpha,\beta)\cos\alpha\xi\sin\beta\eta + g_{sc}(\alpha,\beta)\sin\alpha\xi\cos\beta\eta + g_{ss}(\alpha,\beta)\sin\alpha\xi\sin\beta\eta]\exp[\mp\zeta(\alpha,\beta)z_a]\,d\alpha\,d\beta \quad z \gtrless 0 \quad (3b)$$

where the intrinsic admittance Y_0 is included with A_x^d and A_y^d for convenience. The tangential components of the magnetic

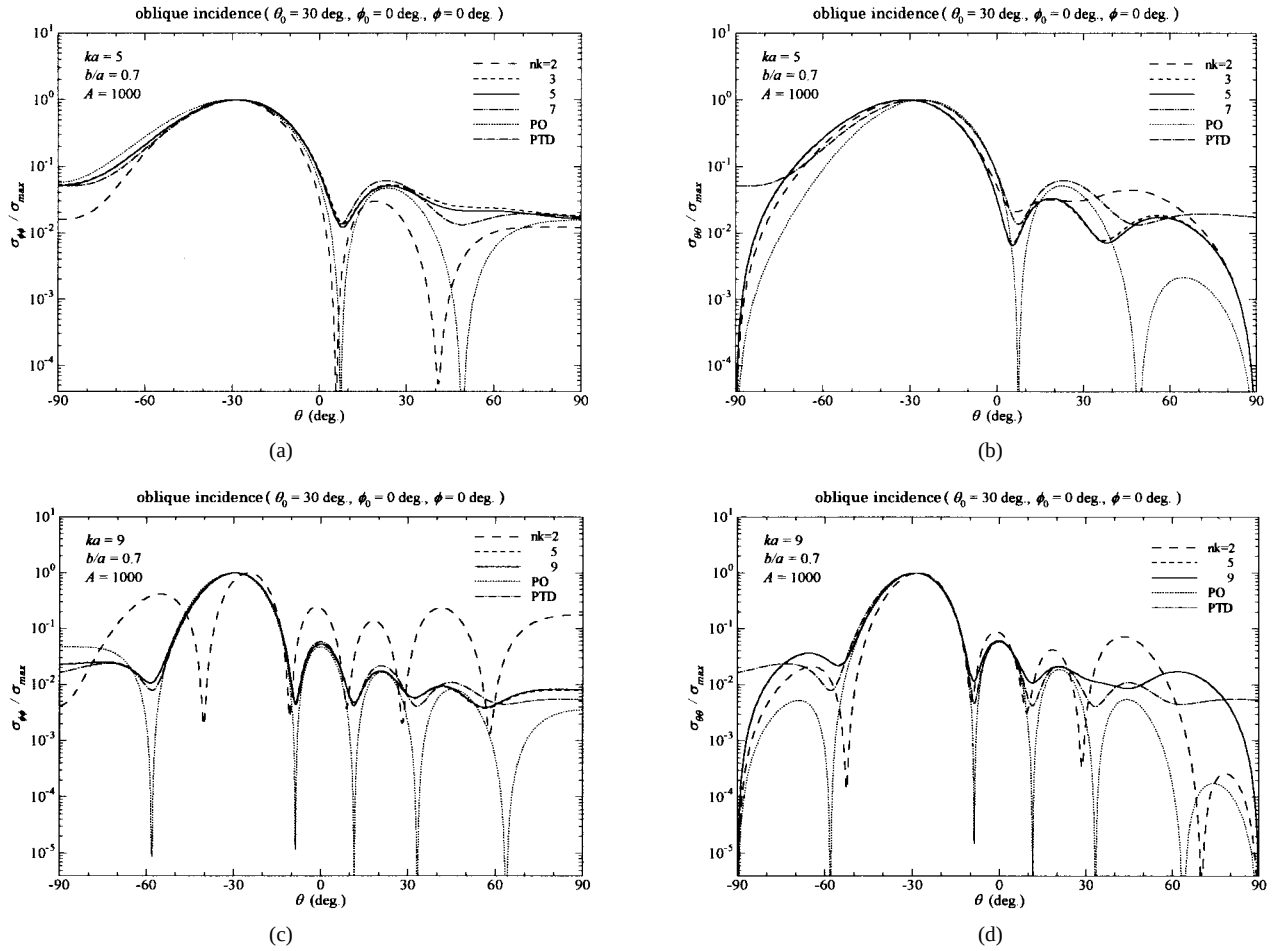

Fig. 4. Far-field pattern diffracted by a perfectly conducting rectangular plate for oblique incidence ($\theta_0 = 30^\circ, \phi_0 = 0^\circ$). Observation point lies in $\phi = 0^\circ$ plane. Plate is $\kappa = ka = 5$ for (a) and (b) and $\kappa = 9$ for (c) and (d). First subscript of σ denotes diffracted field component and second subscript denotes incident wave polarization.

and electric vector potentials are symmetric and antisymmetric with respect to z, respectively. This is because the tangential components of the electric field and the z component of the magnetic fields must be continuous at the plane $z = 0$. The symbols in the above equation are defined by

$$\zeta(\alpha,\beta) = \sqrt{\alpha^2 + p^2\beta^2 - \kappa^2}, \quad \xi = \frac{x}{a}, \quad \eta = \frac{y}{b}$$
$$z_a = \frac{z}{a}, \quad p = \frac{a}{b}, \quad q = \frac{b}{a}, \quad \kappa = ka. \tag{3c}$$

The integrands are the elementary solutions to the 3-D wave equation in a Cartesian coordinate system. The functions $f(\alpha,\beta)$ and $g(\alpha,\beta)$ are unknown and are determined from the required boundary conditions described below.

1) Conducting Plate: The tangential components of the diffracted magnetic field given by

$$H_x^s = -\frac{1}{\mu}\frac{\partial A_y^d}{\partial z}, \quad H_y^s = \frac{1}{\mu}\frac{\partial A_x^d}{\partial z} \tag{4a}$$

must be continuous on the extension of the plate ($|x| > a,\ |y| > b,\ z = 0$) and

$$E_x^i + E_x^s = 0, \quad E_y^i + E_y^s = 0 \tag{4b}$$

on the plate ($|x| < a,\ |y| < b, z = 0$). In addition to the boundary condition, we seek the solution in which H_x and H_y behave like

$$H_x \sim (a^2 - x^2)^{-\frac{1}{2}}(b^2 - y^2)^{\frac{1}{2}}$$
$$H_y \sim (a^2 - x^2)^{\frac{1}{2}}(b^2 - y^2)^{-\frac{1}{2}} \tag{4c}$$

near the edge of the plate.

2) Hole: The tangential components of the diffracted electric field must vanish on the plate ($|x| > a,\ |y| > b,\ z = 0$); that is

$$E_x^d = \frac{1}{\epsilon}\frac{\partial F_y^d}{\partial z} = 0, \quad E_y^d = -\frac{1}{\epsilon}\frac{\partial F_x^d}{\partial z} = 0 \tag{5a}$$

and the tangential components of the total magnetic field must be continuous on the aperture ($|x| < a,\ |y| < b,\ z = 0$)

$$H_x^i + H_x^r + H_x^{d+} = H_x^{d-}, \quad H_y^i + H_y^r + H_y^{d+} = H_y^{d-}. \tag{5b}$$

The edge condition corresponding to (4c) is given by

$$E_x \sim (a^2 - x^2)^{-\frac{1}{2}}(b^2 - y^2)^{\frac{1}{2}}$$
$$E_y \sim (a^2 - x^2)^{\frac{1}{2}}(b^2 - y^2)^{-\frac{1}{2}}. \tag{5c}$$

By imposing the conditions (4a) and (4b) for the plate and (5a) and (5b) for the hole on the vector potentials of (3), we obtain the dual integral equations for the weighting functions $f(\alpha,\beta)$ and $g(\alpha,\beta)$.

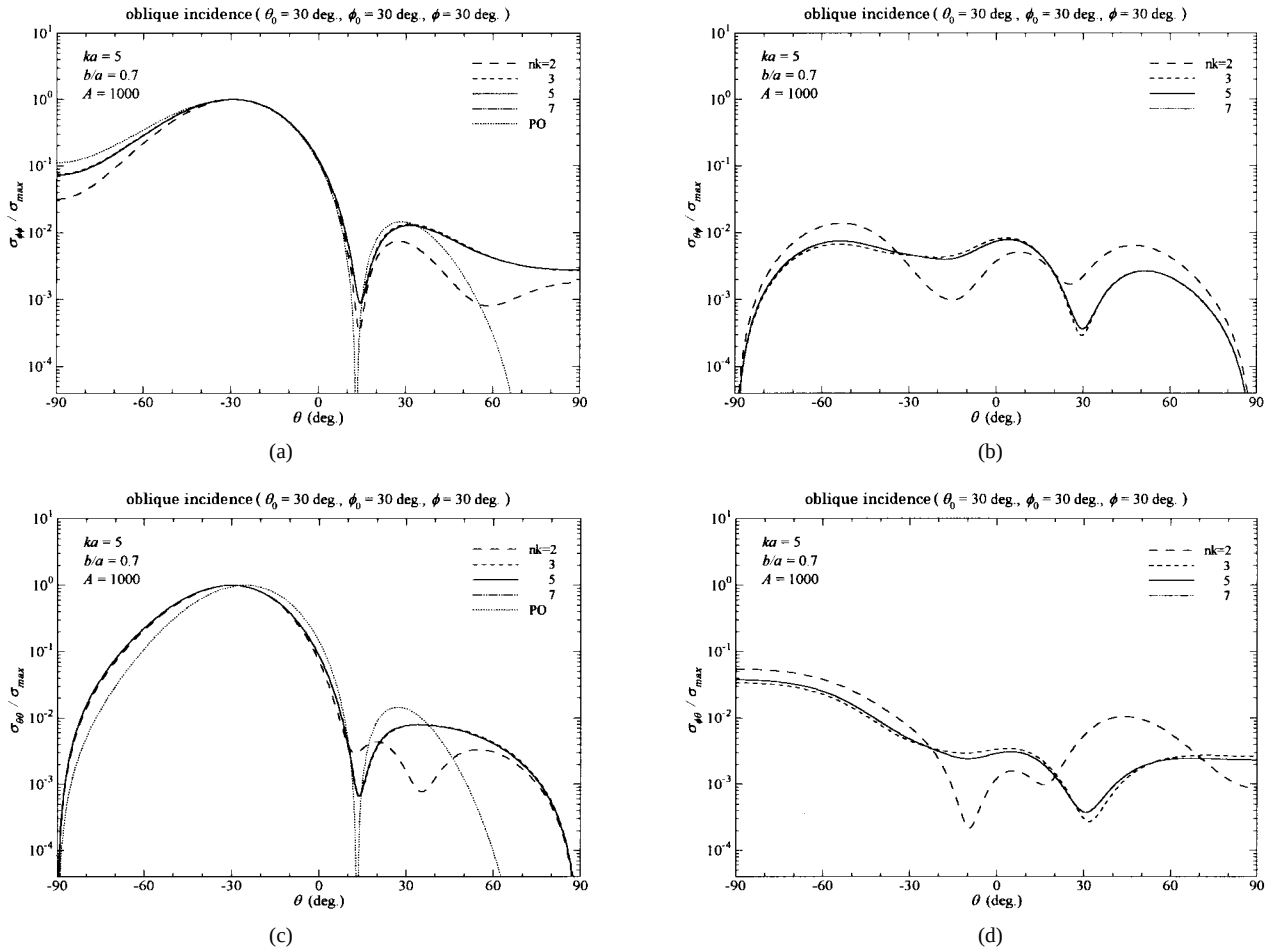

Fig. 5. Far-field pattern diffracted by a perfectly conducting rectangular plate for oblique incidence ($\theta_0 = 30°, \phi_0 = 30°$). Plate is $\kappa = ka = 5$ for (a)–(d). First subscript of σ denotes diffracted field component and second subscript denotes incident wave polarization.

3) Matrix Equation: The solution to the equation associated with (4a) and (5a) can be obtained using the properties of the Weber–Schafheitlin's integrals defined by

$$W(\mu,\nu,\lambda;u) = \int_0^\infty \frac{J_\mu(u\xi)J_\nu(\xi)}{\xi^\lambda}\,d\xi$$
$$= \frac{u^\mu \Gamma\left[\frac{1}{2}(\mu+\nu+1-\lambda)\right]}{2^\lambda \Gamma(\mu+1)\Gamma\left[\frac{1}{2}(-\mu+\nu+1+\lambda)\right]} \times F\left[\frac{\mu+\nu+1-\lambda}{2}, \frac{\mu-\nu+1-\lambda}{2}, \mu+1; u^2\right] \quad (0 \le u < 1)$$
$$= \frac{\Gamma\left[\frac{1}{2}(\mu+\nu+1-\lambda)\right]}{2^\lambda u^{\nu+1-\lambda}\Gamma(\nu+1)\Gamma\left[\frac{1}{2}(\mu-\nu+1+\lambda)\right]} \times F\left[\frac{\mu+\nu+1-\lambda}{2}, \frac{-\mu+\nu+1-\lambda}{2}, \nu+1; \frac{1}{u^2}\right] \quad (u > 1) \quad (6)$$

where $J_\mu(x)$ is the Bessel function of order μ and argument x, $F(a,b,c;x)$ is the hypergeometric function, and $\Gamma(x)$ is the Gamma function. The derivation of the above relation is discussed in [18]. It is known that $W(\mu,\nu,\lambda,u) \equiv 0$ for $u > 1$ when the relation $\mu-\nu+\lambda+1 = -2n$, $(n = 0, 1, 2, \cdots)$ holds. At this step, we incorporate the edge conditions of (4c) and (5c) by selecting appropriate relations among the orders μ, ν and index λ. The unknown functions $f(\alpha,\beta)$ and $g(\alpha,\beta)$ are determined using these properties. The resulting expressions are given by

$$\begin{pmatrix} A_x^d \\ F_x^d \end{pmatrix} = a\begin{pmatrix} \mu Y_0 \\ \mp\epsilon \end{pmatrix} \sum_{m=0}^\infty \sum_{n=0}^\infty \int_0^\infty \int_0^\infty \frac{1}{\zeta(\alpha,\beta)} \times \frac{1}{\alpha}\Big\{J_{2m+1}(\alpha)\cos\alpha\xi\big[A_{mn}^{(x)}J_{2n}(\beta)\cos\beta\eta + B_{mn}^{(x)}J_{2n+1}(\beta)\sin\beta\eta\big] + J_{2m+2}(\alpha) \times \sin\alpha\xi\big[C_{mn}^{(x)}J_{2n}(\beta)\cos\beta\eta + D_{mn}^{(x)}J_{2n+1}(\beta)\sin\beta\eta\big]\Big\}\exp[\mp\zeta(\alpha,\beta)z_a]\,d\alpha\,d\beta \quad (7a)$$

$$\begin{pmatrix} A_y^d \\ F_y^d \end{pmatrix} = a\begin{pmatrix} \mu Y_0 \\ \mp\epsilon \end{pmatrix} \sum_{m=0}^\infty \sum_{n=0}^\infty \int_0^\infty \int_0^\infty \frac{1}{\zeta(\alpha,\beta)} \times \frac{1}{\beta}\Big\{J_{2m}(\alpha)\cos\alpha\xi\big[A_{mn}^{(y)}J_{2n+1}(\beta)\cos\beta\eta + B_{mn}^{(y)}J_{2n+2}(\beta)\sin\beta\eta\big] + J_{2m+1}(\alpha) \times \sin\alpha\xi\big[C_{mn}^{(y)}J_{2n+1}(\beta)\cos\beta\eta + D_{mn}^{(y)}J_{2n+2}(\beta)\sin\beta\eta\big]\Big\}\exp[\mp\zeta(\alpha,\beta)z_a]\,d\alpha\,d\beta \quad (7b)$$

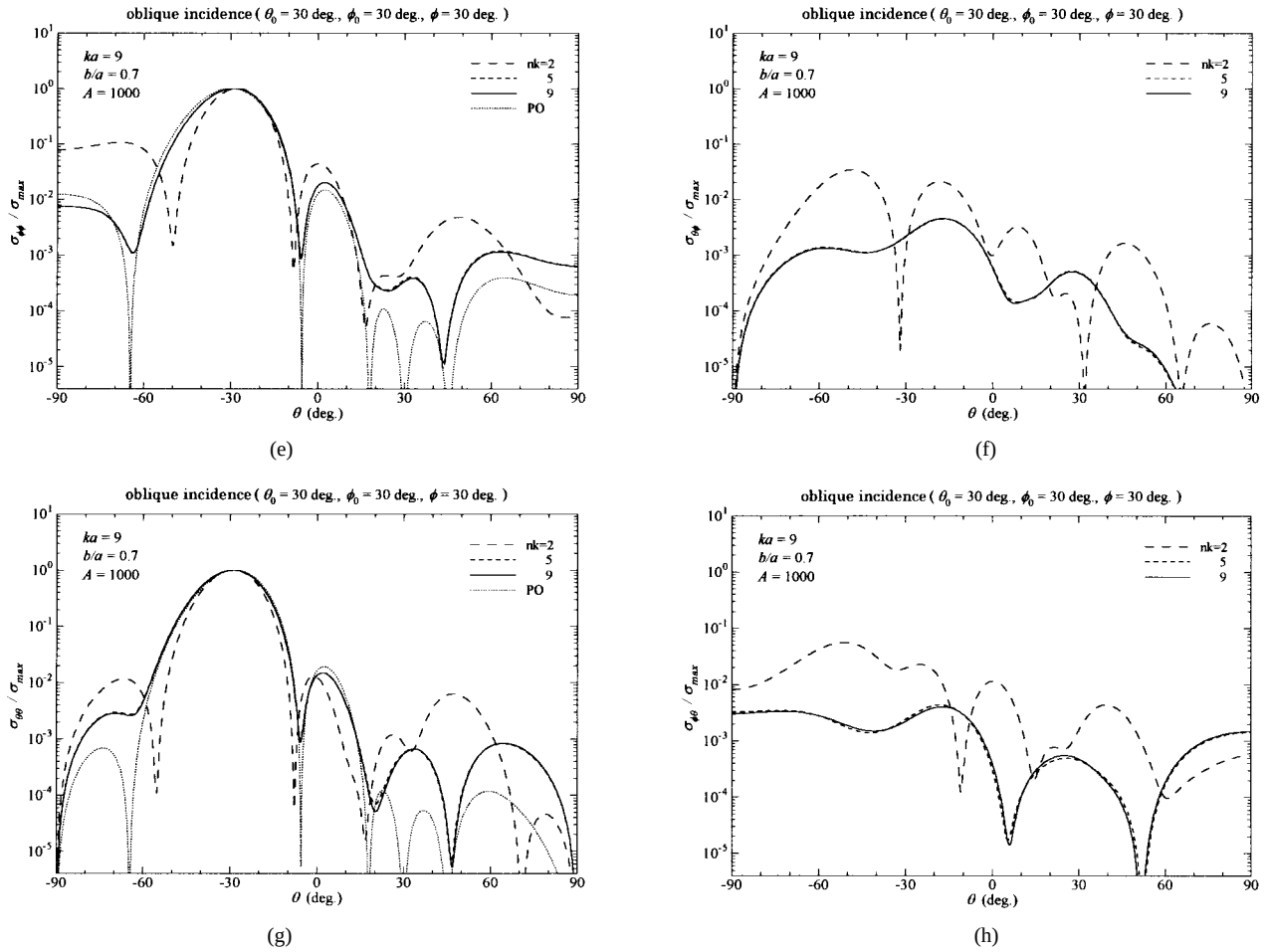

Fig. 5. (*Continued.*) Far-field pattern diffracted by a perfectly conducting rectangular plate for oblique incidence ($\theta_0 = 30°, \phi_0 = 30°$). Plate is $\kappa = 9$ for (e)–(h). First subscript of σ denotes diffracted field component and second subscript denotes incident wave polarization.

where the relations between the trigonometric and Bessel functions

$$\cos x = \sqrt{\frac{\pi x}{2}} J_{-\frac{1}{2}}(x), \quad \sin x = \sqrt{\frac{\pi x}{2}} J_{\frac{1}{2}}(x)$$

are used when we impose the boundary and edge conditions on the expressions in (3). We do not give the explicit expressions of $f(\alpha,\beta)$ and $g(\alpha,\beta)$ as these are readily obtained by comparing (7) and (3).

Imposing the boundary conditions on the conducting plate so that the tangential components of the total electric field vanish, we have the following relations:

$$\begin{aligned}
&\sum_{m=0}^{\infty}\sum_{n=0}^{\infty}\int_0^{\infty}\int_0^{\infty}\frac{(\kappa^2-\alpha^2)}{\zeta(\alpha,\beta)}\\
&\times\frac{1}{\alpha}\{J_{2m+1}(\alpha)\cos\alpha\xi\big[A_{mn}^{(x)}J_{2n}(\beta)\cos\beta\eta\\
&+B_{mn}^{(x)}J_{2n+1}(\beta)\sin\beta\eta\big]+J_{2m+2}(\alpha)\sin\alpha\xi\\
&\times\big[C_{mn}^{(x)}J_{2n}(\beta)\cos\beta\eta+D_{mn}^{(x)}J_{2n+1}(\beta)\sin\beta\eta\big]\}\,d\alpha\,d\beta\\
&+p\sum_{m=0}^{\infty}\sum_{n=0}^{\infty}\int_0^{\infty}\int_0^{\infty}\frac{\alpha}{\zeta(\alpha,\beta)}\{J_{2m}(\alpha)\sin\alpha\xi\big[A_{mn}^{(y)}J_{2n+1}(\beta)\\
&\times\sin\beta\eta-B_{mn}^{(y)}J_{2n+2}(\beta)\cos\beta\eta\big]+J_{2m+1}(\alpha)\cos\alpha\xi\\
&\times\big[-C_{mn}^{(y)}J_{2n+1}(\beta)\sin\beta\eta+D_{mn}^{(y)}J_{2n+2}(\beta)\cos\beta\eta\big]\}\,d\alpha\,d\beta\\
&=-jP_x\exp[jk(x\sin\theta_0\cos\phi_0+y\sin\theta_0\sin\phi_0)] \qquad (8a)
\end{aligned}$$

$$\begin{aligned}
&q\sum_{m=0}^{\infty}\sum_{n=0}^{\infty}\int_0^{\infty}\int_0^{\infty}\frac{\beta}{\zeta(\alpha,\beta)}\{J_{2m+1}(\alpha)\sin\alpha\xi\\
&\times\big[A_{mn}^{(x)}J_{2n}(\beta)\sin\beta\eta-B_{mn}^{(x)}J_{2n+1}(\beta)\cos\beta\eta\big]\\
&+J_{2m+2}(\alpha)\cos\alpha\xi\big[-C_{mn}^{(x)}J_{2n}(\beta)\sin\beta\eta\\
&+D_{mn}^{(x)}J_{2n+1}(\beta)\cos\beta\eta\big]\}\,d\alpha\,d\beta\\
&+\sum_{m=0}^{\infty}\sum_{n=0}^{\infty}\int_0^{\infty}\int_0^{\infty}\frac{(q^2\kappa^2-\beta^2)}{\zeta(\alpha,\beta)}\frac{1}{\beta}\{J_{2m}(\alpha)\cos\alpha\xi\\
&\times\big[A_{mn}^{(y)}J_{2n+1}(\beta)\cos\beta\eta+B_{mn}^{(y)}J_{2n+2}(\beta)\sin\beta\eta\big]\\
&+J_{2m+1}(\alpha)\sin\alpha\xi\big[C_{mn}^{(y)}J_{2n+1}(\beta)\cos\beta\eta\\
&+D_{mn}^{(y)}J_{2n+2}(\beta)\sin\beta\eta\big]\}\,d\alpha\,d\beta\\
&=-jq^2P_y\exp[jk(x\sin\theta_0\cos\phi_0+y\sin\theta_0\sin\phi_0)]. \qquad (8b)
\end{aligned}$$

Similar equations are derived for the rectangular hole. When the concept of projection is applied, the Jacobi's polynomials defined by [20]

$$\begin{aligned}
G_n(\alpha,\gamma,x) = \frac{\Gamma(\gamma)}{\Gamma(\gamma+n)}x^{1-\gamma}(1-x)^{\gamma-\alpha}\frac{d^n}{dx^n}\\
\times\{x^{n+\gamma-1}(1-x)^{\alpha+n-\gamma}\}
\end{aligned}$$

with $\alpha = m+\frac{3}{2}$ and $\gamma = m+1$ are used as the expansion and testing functions. These polynomials have the orthogonalities

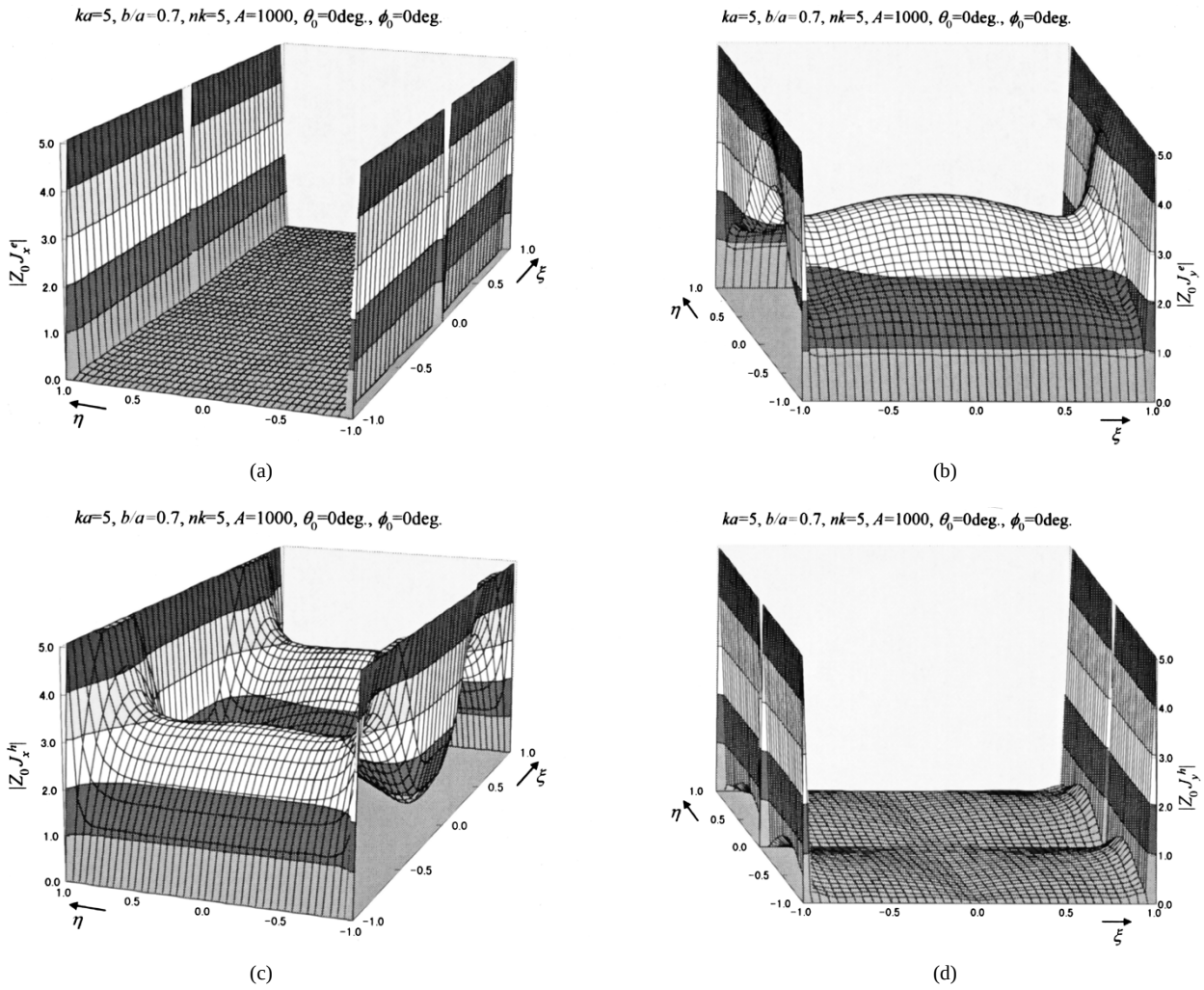

Fig. 6. Distribution of amplitude of current densities J_x and J_y induced on perfectly conducting rectangular plate when plane wave is normally incident. Plate is $\kappa = ka = 5$ for (a)–(d). Superscripts e and h of J denote perpendicular and parallel polarizations of incident wave, respectively.

$$\begin{bmatrix} K_A(2m+1,2n,2s+1,2t+1) & pG_A(2m+1,2n+2,2s+1,2t+1) \\ qG_B(2m+1,2n,2s+2,2t+2) & K_B(2m+1,2n+2,2s+2,2t+2) \end{bmatrix} \times \begin{bmatrix} A_{mn}^{(x)} \\ D_{mn}^{(y)} \end{bmatrix} = \begin{bmatrix} -j\Lambda(\kappa\sin\theta_0\cos\phi_0, 2s+1)\Lambda(q\kappa\sin\theta_0\sin\phi_0, 2t+1)P_x \\ jq^2\Lambda(\kappa\sin\theta_0\cos\phi_0, 2s+2)\Lambda(q\kappa\sin\theta_0\sin\phi_0, 2t+2)P_y \end{bmatrix} \tag{9a}$$

$$\begin{bmatrix} K_A(2m+1,2n+1,2s+1,2t+2) & -pG_A(2m+1,2n+1,2s+1,2t+2) \\ -qG_B(2m+1,2n+1,2s+2,2t+1) & K_B(2m+1,2n+1,2s+2,2t+1) \end{bmatrix} \times \begin{bmatrix} B_{mn}^{(x)} \\ C_{mn}^{(y)} \end{bmatrix} = \begin{bmatrix} \Lambda(\kappa\sin\theta_0\cos\phi_0, 2s+1)\Lambda(q\kappa\sin\theta_0\sin\phi_0, 2t+2)P_x \\ q^2\Lambda(\kappa\sin\theta_0\cos\phi_0, 2s+2)\Lambda(q\kappa\sin\theta_0\sin\phi_0, 2t+1)P_y \end{bmatrix} \tag{9b}$$

$$\begin{bmatrix} K_A(2m+2,2n,2s+2,2t+1) & -pG_A(2m,2n+2,2s+2,2t+1) \\ -qG_B(2m+2,2n,2s+1,2t+2) & K_B(2m,2n+2,2s+1,2t+2) \end{bmatrix} \times \begin{bmatrix} C_{mn}^{(x)} \\ B_{mn}^{(y)} \end{bmatrix} = \begin{bmatrix} \Lambda(\kappa\sin\theta_0\cos\phi_0, 2s+2)\Lambda(q\kappa\sin\theta_0\sin\phi_0, 2t+1)P_x \\ q^2\Lambda(\kappa\sin\theta_0\cos\phi_0, 2s+1)\Lambda(q\kappa\sin\theta_0\sin\phi_0, 2t+2)P_y \end{bmatrix} \tag{9c}$$

$$\begin{bmatrix} K_A(2m+2,2n+1,2s+2,2t+2) & pG_A(2m,2n+1,2s+2,2t+2) \\ qG_B(2m+2,2n+1,2s+1,2t+1) & K_B(2m,2n+1,2s+1,2t+1) \end{bmatrix} \times \begin{bmatrix} D_{mn}^{(x)} \\ A_{mn}^{(y)} \end{bmatrix} = \begin{bmatrix} j\Lambda(\kappa\sin\theta_0\cos\phi_0, 2s+2)\Lambda(q\kappa\sin\theta_0\sin\phi_0, 2t+2)P_x \\ -jq^2\Lambda(\kappa\sin\theta_0\cos\phi_0, 2s+1)\Lambda(q\kappa\sin\theta_0\sin\phi_0, 2t+1)P_y \end{bmatrix}, \tag{9d}$$

$$s = 0, 1, 2, \cdots, \quad t = 0, 1, 2, \cdots$$

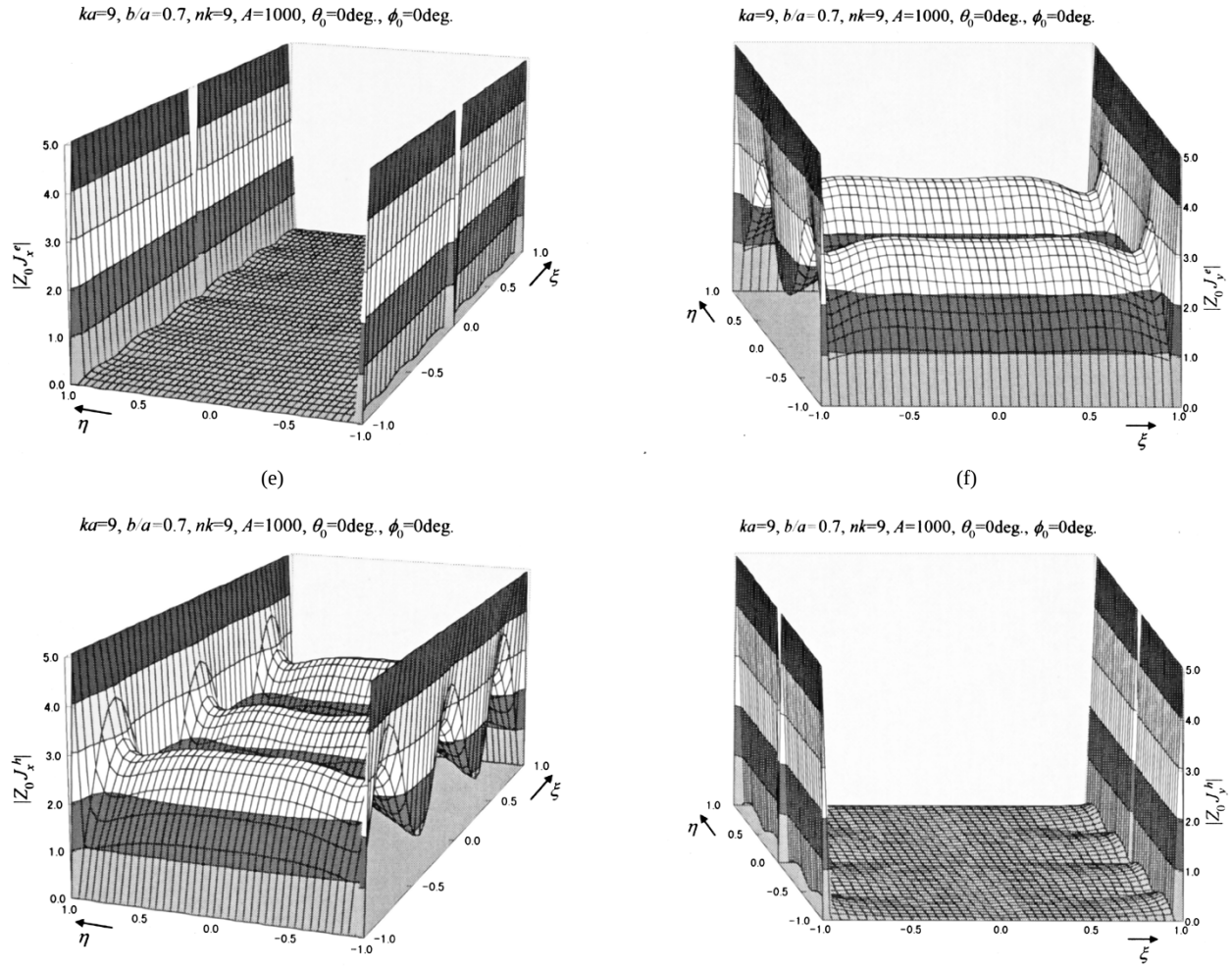

Fig. 6. (*Continued.*) Distribution of amplitude of current densities J_x and J_y induced on perfectly conducting rectangular plate when plane wave is normally incident. Plate is $\kappa = 9$ for (e)–(h). Superscripts e and h of J denote perpendicular and parallel polarizations of incident wave, respectively.

and expansion formula of the Bessel function given by

$$J_\nu(\alpha\xi) = 2\sqrt{2}\,\xi^\nu \sum_{n=0}^{\infty} \frac{\left(2n+\nu+\frac{3}{2}\right)\Gamma\left(n+\nu+\frac{3}{2}\right)}{\Gamma(n+1)\Gamma(\nu+1)} \times \frac{J_{2n+\nu+\frac{3}{2}}(\alpha)}{\alpha^{\frac{3}{2}}} G_n\left(\nu+\frac{3}{2}, \nu+1, \xi^2\right).$$

This is derived by integrating the product of the Bessel function and the Jacobi's polynomials. According to the procedure similar to the MoM, we have the matrix equations for the expansion coefficients, shown at the bottom of the previous page, where

$$P_x = \begin{cases} E_2\kappa\cos\theta_0\cos\phi_0 - E_1\kappa\sin\phi_0 \\ -E_2\kappa\sin\phi_0 - E_1\kappa\cos\theta_0\cos\phi_0 \end{cases}, \quad P_y = \begin{cases} E_2\kappa\cos\theta_0\sin\phi_0 + E_1\kappa\cos\phi_0 \\ E_2\kappa\cos\phi_0 - E_1\kappa\cos\theta_0\sin\phi_0 \end{cases} \quad \begin{pmatrix}\text{Plate}\\ \text{Hole}\end{pmatrix} \tag{10a}$$

$$K_A(m,n,\mu,\nu) = \int_0^\infty\int_0^\infty \frac{\kappa^2-\alpha^2}{\sqrt{\alpha^2+p^2\beta^2-\kappa^2}} \times \frac{J_m(\alpha)J_\mu(\alpha)}{\alpha^2}\frac{J_n(\beta)J_\nu(\beta)}{\beta}\,d\alpha\,d\beta \tag{10b}$$

$$K_B(m,n,\mu,\nu) = \int_0^\infty\int_0^\infty \frac{q^2\kappa^2-\beta^2}{\sqrt{\alpha^2+p^2\beta^2-\kappa^2}} \times \frac{J_m(\alpha)J_\mu(\alpha)}{\alpha}\frac{J_n(\beta)J_\nu(\beta)}{\beta^2}\,d\alpha\,d\beta \tag{10c}$$

$$G_A(m,n,\mu,\nu) = \int_0^\infty\int_0^\infty (\alpha^2+p^2\beta^2-\kappa^2)^{-\frac{1}{2}} J_m(\alpha) \times J_\mu(\alpha)\frac{J_n(\beta)J_\nu(\beta)}{\beta}\,d\alpha\,d\beta \tag{10d}$$

$$G_B(m,n,\mu,\nu) = \int_0^\infty\int_0^\infty (\alpha^2+p^2\beta^2-\kappa^2)^{-\frac{1}{2}} \times \frac{J_m(\alpha)J_\mu(\alpha)}{\alpha} J_n(\beta)J_\nu(\beta)\,d\alpha\,d\beta \tag{10e}$$

$$\Lambda(x,\nu) = \frac{J_\nu(x)}{x}. \tag{10f}$$

Thus, the problem is reduced to the matrix equation for the expansion coefficients. Once the expansion coefficients are determined, electromagnetic fields may be derived from (7). The matrix size is $2(nk)^2 \times 2(nk)^2$, where $nk-1$ is the maximum values of indexes m, n, s, and t. The computation

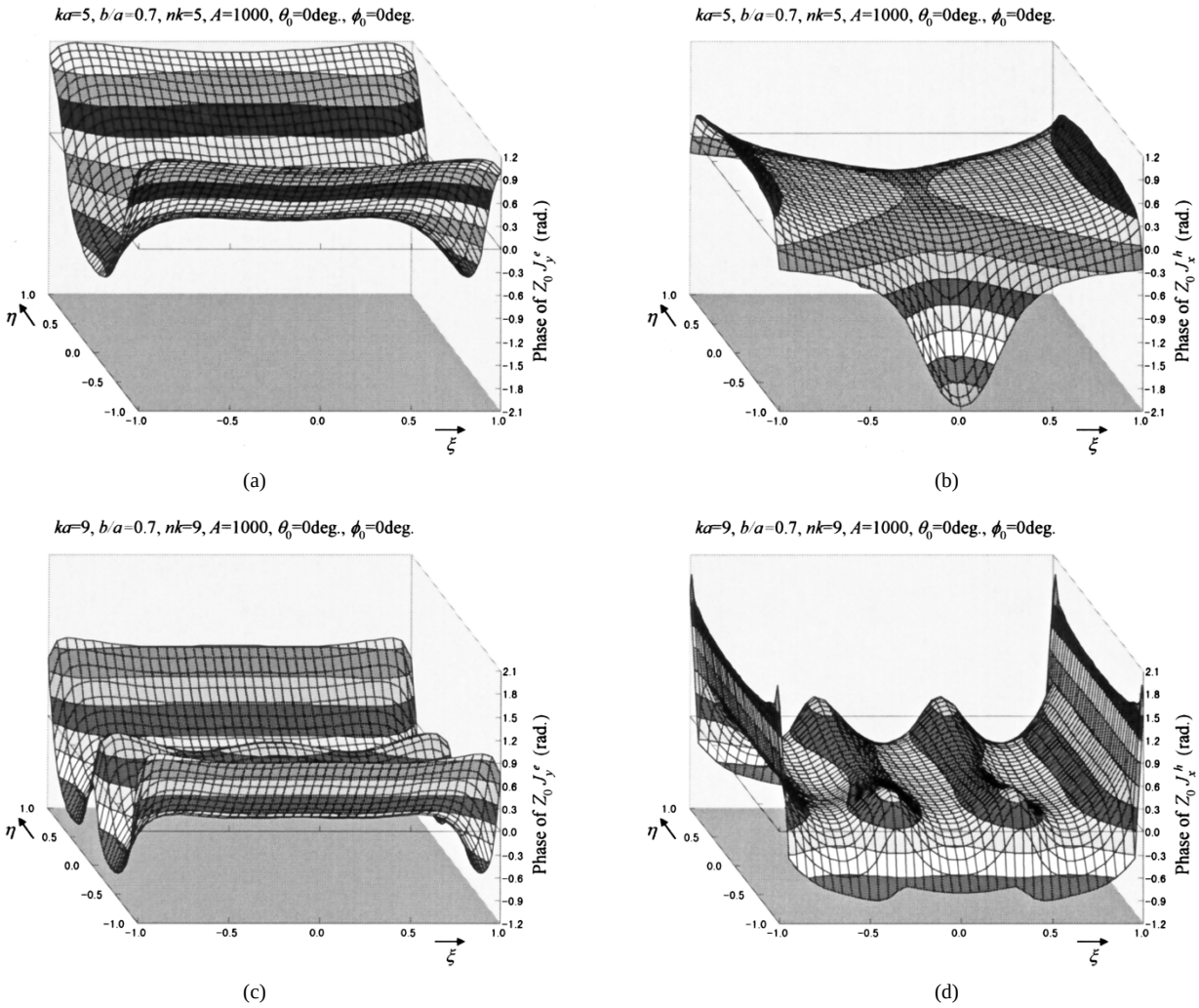

Fig. 7. Distribution of phase of current densities J_x and J_y induced on perfectly conducting rectangular plate when plane wave is normally incident. Plate is $\kappa = ka = 5$ for (a) and (b) and $\kappa = 9$ for (c) and (d). Superscripts e and h of J denote perpendicular and parallel polarizations of incident wave, respectively. Only copolarized components are shown.

of the matrix elements K_A, K_B, G_A, and G_B is not easy since they are double infinite integrals that converge rather slowly. The computation of these integrals is discussed in [11].

B. Field Distribution

The current density **J** induced on the perfectly conducting rectangular plate and the electric field distribution **E** on the rectangular aperture are obtained from the vector potentials given in (7). The integration over the variables α and β can be performed since the integrals are special forms of the Weber–Schafheitlin's discontinuous integrals [18]–[20]; the result is given by

$$\begin{pmatrix} J_x \\ E_y \end{pmatrix} = \begin{pmatrix} 2Y_0 \\ -1 \end{pmatrix} \frac{\sqrt{1-\xi^2}}{\sqrt{1-\eta^2}} \sum_{m=0}^{\infty}\sum_{n=0}^{\infty}(-1)^{m+n} \times \left\{ \left[A_{mn}^{(x)} T_{2n}(\eta) + B_{mn}^{(x)} T_{2n+1}(\eta)\right] \frac{U_{2m}(\xi)}{2m+1} + \left[C_{mn}^{(x)} T_{2n}(\eta) + D_{mn}^{(x)} T_{2n+1}(\eta)\right] \frac{U_{2m+1}(\xi)}{2m+2} \right\} \tag{11a}$$

$$\begin{pmatrix} J_y \\ E_x \end{pmatrix} = \begin{pmatrix} 2Y_0 \\ 1 \end{pmatrix} \frac{\sqrt{1-\eta^2}}{\sqrt{1-\xi^2}} \sum_{m=0}^{\infty}\sum_{n=0}^{\infty}(-1)^{m+n} \times \left\{ \left[A_{mn}^{(y)} \frac{U_{2n}(\eta)}{2n+1} + B_{mn}^{(y)} \frac{U_{2n+1}(\eta)}{2n+2}\right] T_{2m}(\xi) + \left[C_{mn}^{(y)} \frac{U_{2n}(\eta)}{2n+1} + D_{mn}^{(y)} \frac{U_{2n+1}(\eta)}{2n+2}\right] T_{2m+1}(\xi) \right\} \tag{11b}$$

where $T_n(x)$ and $U_n(x)$ are Chebyshev polynomials of the first and second kinds, respectively. From the above equations, J_x and E_y are proportional to $(1-\xi^2)^{\frac{1}{2}}(1-\eta^2)^{-\frac{1}{2}}$ and J_y and E_x are proportional to $(1-\xi^2)^{-\frac{1}{2}}(1-\eta^2)^{\frac{1}{2}}$. These variables are consistent with the required edge conditions for the field components.

C. Far Field

Vector potentials of (7) are transformed into the form

$$I = \int_{-\infty}^{\infty}\int_{-\infty}^{\infty} Q(\alpha,\beta) \cdot \exp\left[-j(\alpha\xi+\beta\eta)\sqrt{\frac{\alpha^2}{a^2}+\frac{\beta^2}{b^2}-k^2}z\right] d\alpha\, d\beta. \tag{12a}$$

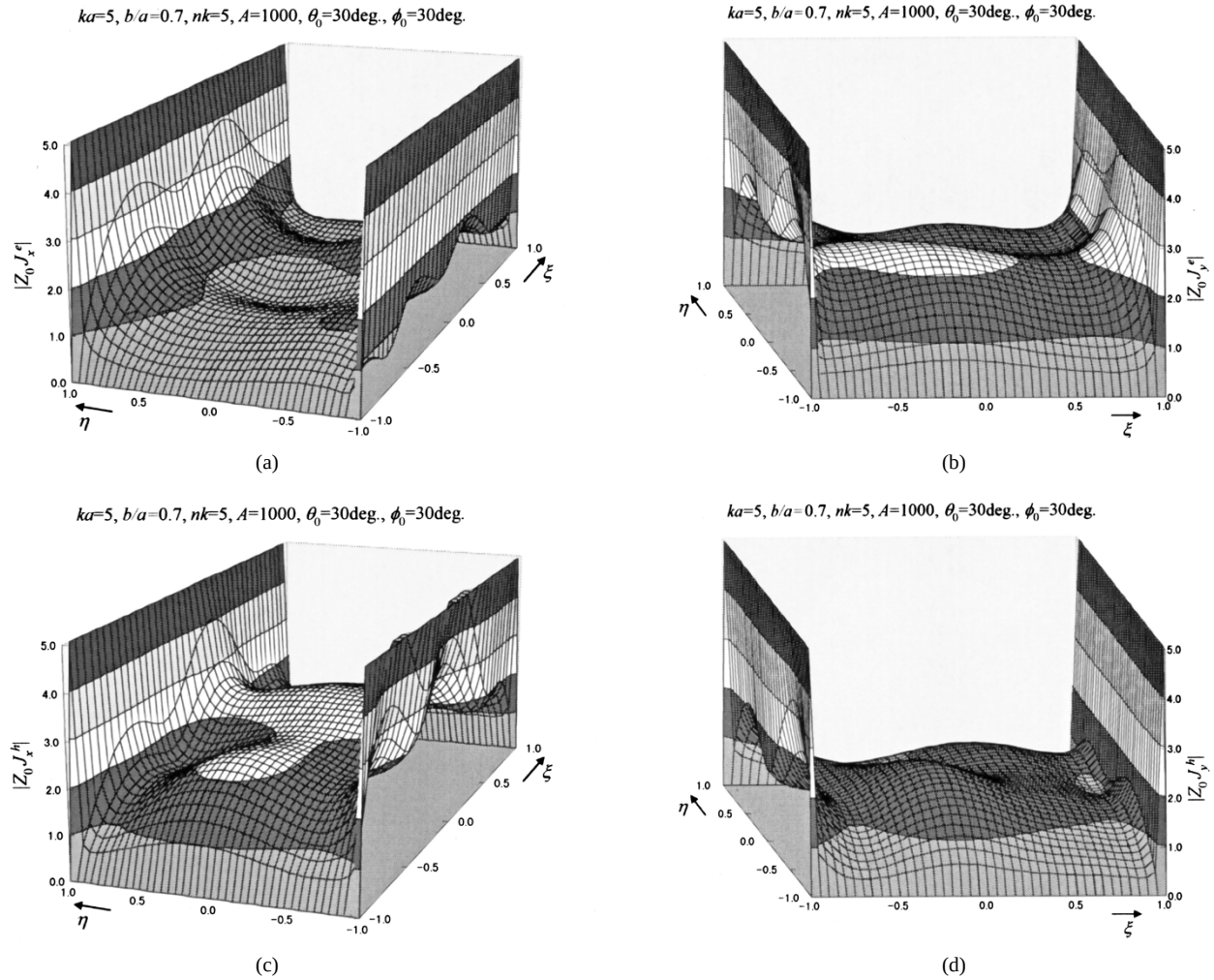

Fig. 8. Distribution of amplitude of current densities J_x and J_y induced on perfectly conducting rectangular plate when plane wave is obliquely incident ($\theta_0 = 30^\circ, \phi_0 = 30^\circ$). Plate is $\kappa = ka = 5$. Superscripts e and h of J denote perpendicular and parallel polarizations of incident wave, respectively.

Using the transformation of the variables

$$\frac{\alpha}{a} = k\sin\gamma\cos\delta, \quad \frac{\beta}{b} = k\sin\gamma\sin\delta$$
$$x = r\sin\theta\cos\phi, \quad y = r\sin\theta\sin\phi, \quad z = r\cos\theta \tag{12b}$$

and applying the method of the steepest descent, we have

$$\begin{aligned} I &= q\kappa^2 \int_{C_1}\int_{C_2} \tilde{Q}(\gamma,\delta)\exp\{-jkr[\sin\theta\sin\gamma\cos(\phi-\delta) \\ &\quad + \cos\theta\cos\gamma]\}\sin\gamma\cos\gamma\, d\gamma\, d\delta \\ &= j2\pi qka^2 Q(ka\sin\theta\cos\phi, kb\sin\theta\sin\phi) \\ &\quad \times \cos\theta\frac{\exp(-jkr)}{r} \end{aligned} \tag{12c}$$

where $\tilde{Q}(\gamma,\delta) = Q(\alpha,\beta)$, the contours C_1 (γ-plane) and C_2 (δ-plane) are given by $C_1 : [-\frac{1}{2}\pi - j\infty, \frac{1}{2}\pi + j\infty]$ and $C_2 : [0, 2\pi]$. As a result, the far-field expressions of the vector potentials become

$$\begin{aligned} \begin{pmatrix} A_x^d \\ F_x^d \end{pmatrix} &= \begin{pmatrix} Y_0\mu \\ -\epsilon \end{pmatrix}\frac{\pi qa^2}{2}\frac{\exp(-jkr)}{r}\sum_{m=0}^{\infty}\sum_{n=0}^{\infty} \\ &\quad \times \left\{ \frac{J_{2m+1}(ka\sin\theta\cos\phi)}{ka\sin\theta\cos\phi}\left[A_{mn}^{(x)}J_{2n}(kb\sin\theta\sin\phi)\right.\right. \\ &\quad \left. + jB_{mn}^{(x)}J_{2n+1}(kb\sin\theta\sin\phi)\right] \\ &\quad + \frac{J_{2m+2}(ka\sin\theta\cos\phi)}{ka\sin\theta\cos\phi}\left[jC_{mn}^{(x)}J_{2n}(kb\sin\theta\sin\phi)\right. \\ &\quad \left.\left. - D_{mn}^{(x)}J_{2n+1}(kb\sin\theta\sin\phi)\right]\right\} \end{aligned} \tag{13a}$$

$$\begin{aligned} \begin{pmatrix} A_y^d \\ F_y^d \end{pmatrix} &= \begin{pmatrix} Y_0\mu \\ -\epsilon \end{pmatrix}\frac{\pi qa^2}{2}\frac{\exp(-jkr)}{r}\sum_{m=0}^{\infty}\sum_{n=0}^{\infty} \\ &\quad \times \left\{ \frac{J_{2n+1}(kb\sin\theta\sin\phi)}{kb\sin\theta\sin\phi}\left[A_{mn}^{(y)}J_{2m}(ka\sin\theta\cos\phi)\right.\right. \\ &\quad \left. + jC_{mn}^{(y)}J_{2m+1}(ka\sin\theta\cos\phi)\right] \\ &\quad + \frac{J_{2n+2}(kb\sin\theta\sin\phi)}{kb\sin\theta\sin\phi}\left[jB_{mn}^{(y)}J_{2m}(ka\sin\theta\cos\phi)\right. \\ &\quad \left.\left. - D_{mn}^{(y)}J_{2m+1}(ka\sin\theta\cos\phi)\right]\right\}. \end{aligned} \tag{13b}$$

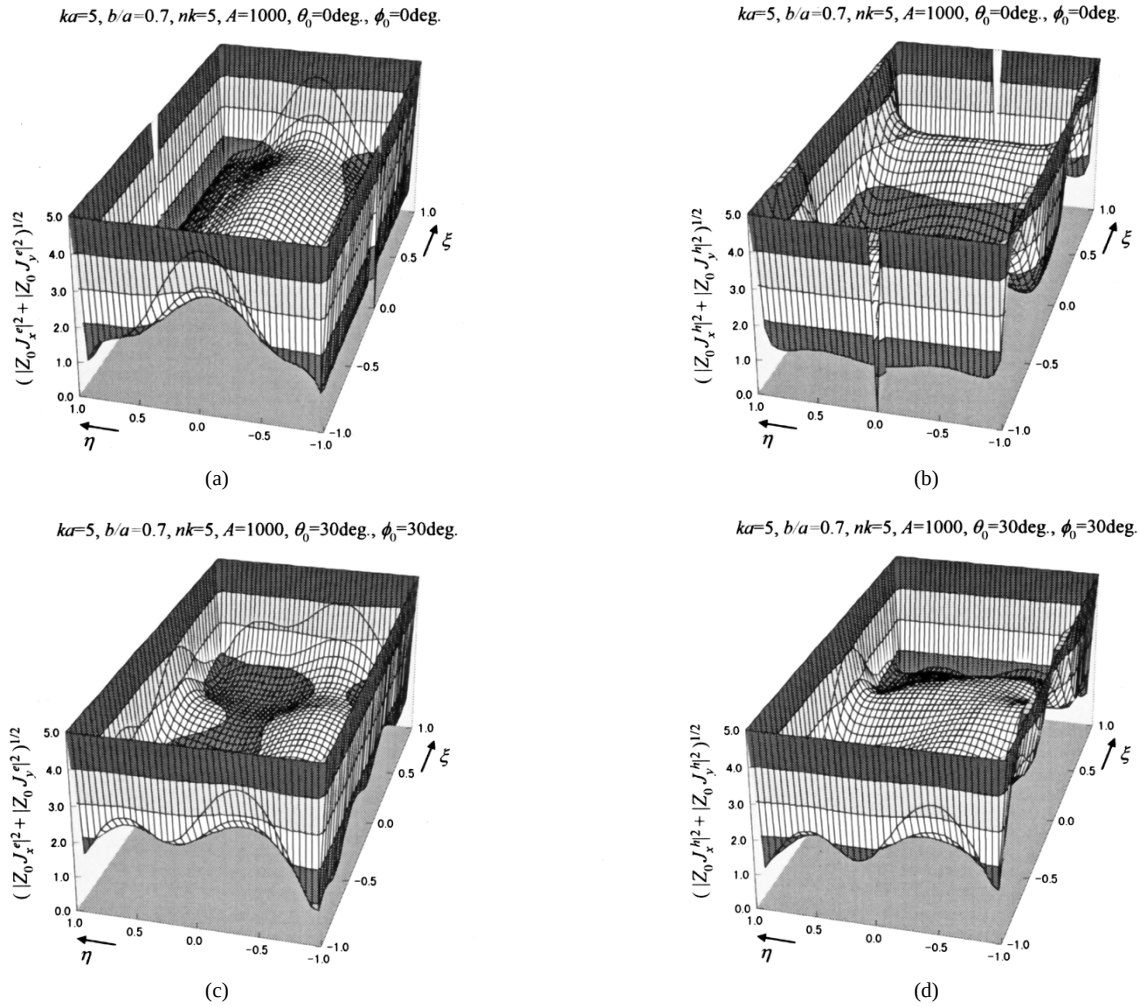

Fig. 9. Distribution of modulus of current density $\sqrt{|J_x|^2+|J_y|^2}$ induced on perfectly conducting rectangular plate when plane wave is normally and obliquely incident. Plate is $\kappa = ka = 5$. (a) and (b) Normal incidence $(\theta_0 = 0^\circ, \phi_0 = 0^\circ)$. (c) and (d) Oblique incidence $(\theta_0 = 30^\circ, \phi_0 = 30^\circ)$. Superscripts e and h of J denote perpendicular and parallel polarizations of incident wave, respectively.

In the far region, the relation between the electric field and the vector potential becomes

$$\begin{aligned} E_\theta &\simeq -j\omega A_\theta = -j\omega\cos\theta(A_x\cos\phi + A_y\sin\phi) \\ E_\theta &\simeq -j\frac{k}{\epsilon}F_\phi = j\frac{k}{\epsilon}(F_x\sin\phi - F_y\cos\phi) \\ E_\phi &\simeq -j\omega(-A_x\sin\phi + A_y\cos\phi) \\ E_\phi &\simeq j\frac{k}{\epsilon}\cos\theta(F_x\cos\phi + F_y\sin\phi). \end{aligned} \tag{14}$$

These fields satisfy the radiation condition.

IV. Computation and Discussion

A. Computations of the Matrix Elements

A first step in obtaining numerical results of physical quantities is to compute the matrix elements defined in (10). These are double infinite integrals that converge rather slowly. The method of computations in this paper is summarized as follows. The full range of integration is divided into several subregions consisting of annular sectors with different radii, as shown in Fig. 2. The numerical integration of these annular sectors is carried out using the Gauss Legendre quadrature scheme. The region exterior to the maximum sector with radius A is divided into three subregions. The integrations of the variables including infinity are performed analytically with asymptotic approximations of the integrands. Hence, double infinite integrals are transformed into the finite double and single integrals plus analytical expressions. The choice of the A value depends on the maximum order $2nk$ of the Bessel functions included in the integrands of the matrix elements. In addition, the variation of A serves partly to verify the validity of the computation since the results of the matrix elements should not depend on the choice of A (details are discussed in [11]).

B. Radiation Pattern

The radiation pattern is computed using (13) and (14) according to the following procedure. First, the matrix elements $K_{A,B}(m,n,s,t)$ and $G_{A,B}(m,n,s,t)$ are calculated for various values of $m,\ n,\ s$ and t up to $nk-1$ with the method of Section IV-A. The matrix size is $2(nk)^2 \times 2(nk)^2$. Once the numerical results for the expansion coefficients are obtained, the radiation patterns are computed from (13) and (14). The numerical results of the far-field pattern diffracted by a perfectly conducting plate for normal incidence are shown in Fig. 3. The plate size is $ka = 5$ for (a)–(d) and $ka = 9$ for

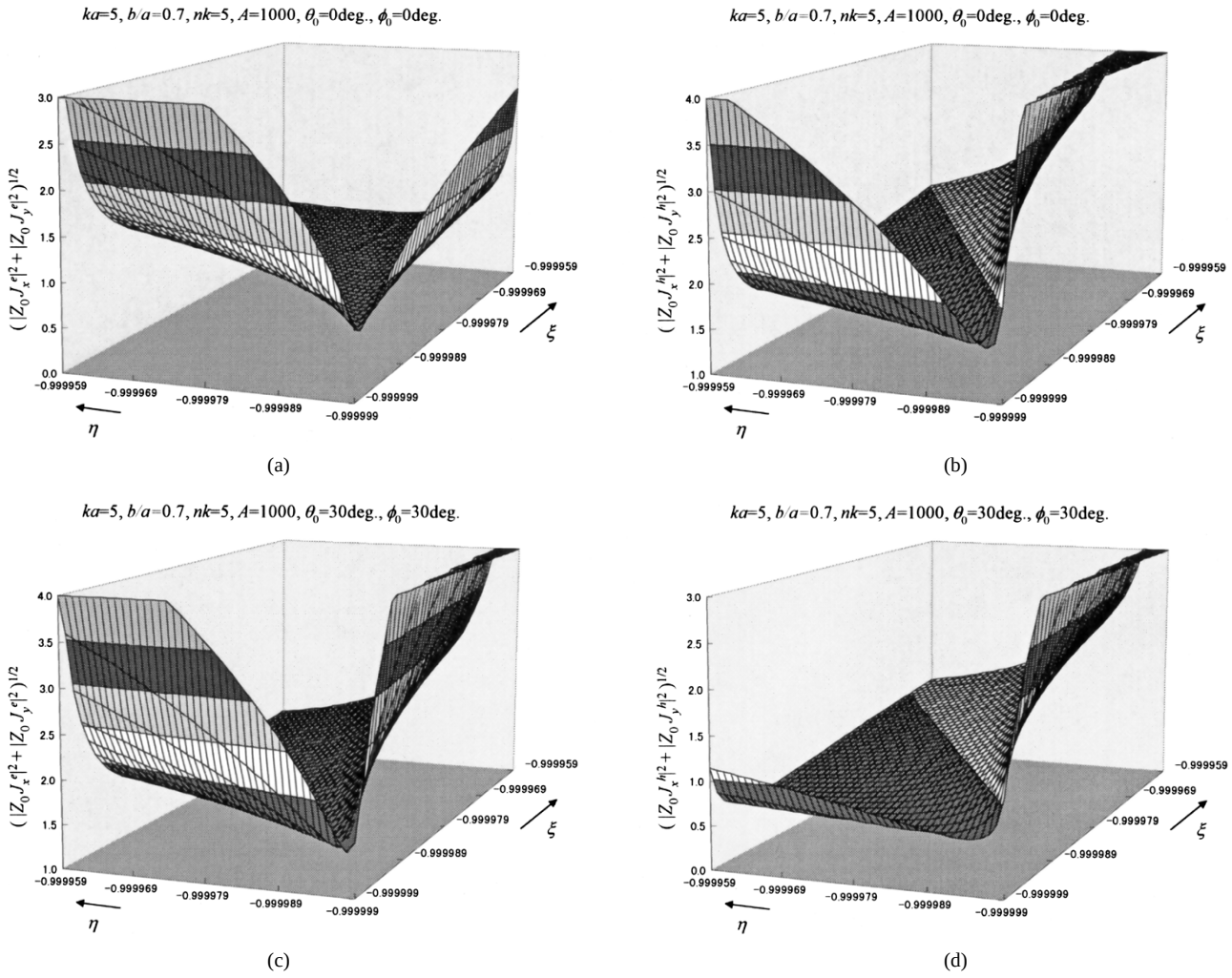

Fig. 10. Enlarged portion of modulus of current densities around vertex.

(e)–(h). The values of $q = b/a$ are fixed to 0.7 in the present computations. The ordinate σ denotes the power pattern or differential scattering cross section. The first subscript of σ represents the component of the diffracted field, while the second subscript refers to the polarization of the incident wave. Copolarized patterns $\sigma_{\theta\theta}$ and $\sigma_{\phi\phi}$ are computed in $\phi = 0°$ plane and cross polarized patterns $\sigma_{\theta\phi}$ and $\sigma_{\phi\theta}$ are computed in $\phi = 90°$ plane. The maximum index nk is varied to see the convergence of the results. As shown in Fig. 3, the results converge with relatively small values of nk, say $nk = 3$ for $ka = 5$ and $nk = 5$ for $ka = 9$. Roughly speaking, solutions converge for $2nk \simeq ka + \alpha$, where α is a small integer that depends on the required precision. This is likely due to the fact that each summand of the expressions of the fields satisfies a part of the required boundary condition as well as the edge condition. As mentioned in Section IV-A, the pattern should be independent of A's value. We computed the patterns for various parameters for $A = 400$ and $A = 1000$. Both results agree completely, but are not shown here to save space. To verify the validity of the present computation, we show the results produced by the physical optics (PO) and physical theory of diffraction (PTD) [21] in these figures. The PTD agrees with the results of the present method even in the sidelobes. A similar trend is seen for oblique incidence ($\theta_0 = 30°$, $\phi_0 = 0°$), as shown in Fig. 4. The plate sizes are $ka = 5$ and $ka = 9$ and the pattern is observed in the cut-pane $\phi = 0°$. Since the plane of incidence and observation point lie in the xz-plane, the PO and PTD patterns are for a 2-D strip. Fig. 5 shows the patterns for oblique incidence ($\theta_0 = 30°, \phi_0 = 30°$)when the cut plane is changed to $\phi = 30°$. Fig. 5(a)–(d) is for $ka = 5$ and Fig. 5(e)–(h) is for $ka = 9$; the results converge for $nk \geq 3$ and $nk \geq 5$, respectively. The rate of the convergence is roughly the same as that with the normal incidence. Since the cross polarized components of the PO solution are zero, they are not shown in the figure. In this figure, a comparison is only made with the PO.

C. Current Densities

In this computation, we discuss the current densities induced on the plate. A similar result is expected for the aperture field distribution. Fig. 6 shows the distribution of current densities J_x and J_y, when the plane wave is normally incident on the plate. Intrinsic impedance Z_0 is multiplied by the current densities since the amplitude of the electric field of the incident wave is assumed to be unified. Fig. 6(a)–(d) is for $ka = 5$ and Fig. 6(e)–(h) is for $ka = 9$. The larger values of nk and A are chosen to obtain more precise results. As

shown in the figure, J_x behaves like $(1-\xi^2)^{\frac{1}{2}}(1-\eta^2)^{-\frac{1}{2}}$ and J_y behaves like $(1-\xi^2)^{-\frac{1}{2}}(1-\eta^2)^{\frac{1}{2}}$. The cross-polarized components of the current densities J_x^e and J_y^h are zero for the PO current approximation, but these are actually produced and undulate up and down around the PO currents as shown in Fig. 6(a), (d), (e), and (h). The amplitude of the J_y^h undulation in the η direction [Fig. 6(d) and (h)] is larger than that of J_x^e in the ξ direction [Fig. 6(a) and (e)]. This is considered to be due to the nearby resonance in the η direction. Fig. 7 shows the corresponding phase distributions (only the copolarized components are shown). The cross-polarized components have rather flat phase distributions in the main portions of the plate and phase jumps along some lines. In addition, they show a complicated distribution near the vertex. We omitted these distributions since the whole profiles are complicated. Fig. 8 shows the current density distributions of oblique incidence for $ka = 5$. In this case, there does not seem to be a distinction between each component.

The modulus of the current density $J = \sqrt{|J_x|^2 + |J_y|^2}$ is also interesting. Fig. 9 shows the distributions of J for normal and oblique incidences. An enlarged figure around the vertex is shown in Fig. 10. J is singular along the edge as expected, however, it remains finite at the vertex regardless of the polarization and incident angle of the incident wave. This is surprising, but we think it is reasonable since each component J_x and J_y becomes the product of zero and infinity at the vertex. Actually, it is not difficult to show that J_x and J_y of (11) approach a finite value in the limit $|\xi| \to 1$ and $|\eta| \to 1$ along the line $(1-|\xi|) = g(1-|\eta|)$ with an arbitrary constant g.

V. Conclusion

We derived the exact solution of the field diffracted by a perfectly conducting rectangular plate and its complementary problem, diffraction by a rectangular hole in a perfectly conducting plate, using the method of the Kobayashi potential. We presented numerical results of the far diffracted field pattern and current distribution on the plate (or aperture field distribution). This method may be regarded as an eigenfunction expansion of the configuration and the convergence was very rapid. The present method promises applicability to a wide class of problems such as radiation from a flanged rectangular waveguide and patch antenna with longitudinal and horizontal sources, diffraction of plane wave by thick rectangular aperture, and so on.

References

[1] C. Huang, R. D. Kodis, and H. Levine, "Diffraction by apertures," *J. Appl. Phys.*, vol. 26, pp. 151–165, 1955.

[2] R. F. Harrington and F. F. Mautz, "Electromagnetic transmission an aperture in a conducting plane," *AEU*, vol. 31, pp. 81–87, 1977.

[3] C. M. Butler and K. R. Umashankar, "Electromagnetic penetration through an aperture in an infinite planar screen separating two half-space of different media," *J. Appl. Phys.*, 1976.

[4] D. I. Kaklamani and N. K. Uzunoglu, "Analysis of dielectrically loaded radiators using entire-domain Galerkin technique," *IEEE Antennas Propagat. Mag.*, vol. 39, pp. 30–54, Oct. 1997.

[5] I. Kobayashi, "Darstellung eines Potentials in zylindrischen Koordinaten, das sich auf einer Ebene innerhalb und ausserhalb einer gewissen Kreisbegrenzung verschiedener Grenzbedingung unterwirft," Sci. Rep., Tohoku Imperial Univ., sendai, Japan, vol. 20, pp. 197–212, 1931.

[6] I. N. Sneddon, *Mixed Boundary Value Problems in Potential Theory*. Amsterdam, The Netherlands: North-Holland, 1966.

[7] Y. Nomura, "The electrostatic problems of two equal parallel circular plates," in *Proc. Phys. Math. Soc. Japan*, 1941, vol. 23, pp. 168–180.

[8] M. Takahashi and K. Hongo, "Capacitance of coupled circular microstrip disks," *IEEE Trans. Microwave Theory Tech.*, vol. MTT-30, pp. 1881–1888, Nov. 1982.

[9] Y. Nomura and N. Kawai, "On the acoustic field by a vibrating source arbitrarily distributed on a plane circular plate," Sci. Rep. Tohoku Univ., Sendai, Japan, vol. 33, no. 4, pp. 197–207, 1949.

[10] T. Otsuki, "Diffraction of an acoustic wave by a rigid rectangular plate," *J. Phys. Soc. Japan*, vol. 19. no. 9, pp. 1733–1741, Sept. 1964.

[11] K. Hongo and H. Sugaya, "Diffraction of an acoustic plane wave by a rectangular plate," *J. Appl. Phys.*, vol. 82, no. 6, pp. 2719–2729, Sept. 15, 1997.

[12] K. Hongo and G. Ishii, "Diffraction of an electromagnetic plane wave by a thick slit," *IEEE Trans. Antennas Propagat.*, vol. AP-26, pp. 494–499, May 1978.

[13] K. Hongo, "Diffraction by a flanged parallel-plate waveguide," *Radio Sci.*, vol. 7, no. 10, pp. 955–963, Oct. 1972.

[14] K. Hongo, N. Furusawa, and H. Hori, "On the two dimensional multiple scattering for N slits array," *Trans. IECE Japan*, vol. 63-B, no. 5, pp. 506–513, 1980 (in Japanese).

[15] Y. Nomura and S. Katsura, "Diffraction of electric waves by circular plate and circular hole," Sci. Rep. Inst. Elect. Commun. Tohoku Univ., vol. 10, pp. 1–26, 1958.

[16] K. Hongo, "Diffraction of an electromagnetic plane wave by circular disk and circular hole," *IEICE Trans. Electron.*, vol. E80-C, no. 11, pp. 1360–1366, Nov. 1997.

[17] K. Hongo and E. Nakajima, "High-frequency diffraction of 2-D scatterers by an incident anisotropic cylindrical wave," *J. Appl. Phys.*, vol. 51, no. 7, pp. 3524–3530, July 1980.

[18] G. N. Watson, *A Treatise on the Theory of Bessel Functions*. Cambridge, MA: Cambridge Univ. Press, 1980, pp. 398–405.

[19] I. S. Gradshteyn and I. M. Rhzhik, *Table of Integrals, Series and Products*. New York: Academic, 1980.

[20] M. Abramowitz and I. A. Stegun, *Handbook of Mathematical Functions*. New York: Dover, 1972.

[21] H. Kobayashi and K. Hongo, "Scattering of electromagnetic plane waves by conducting plates," *Electromagn.*, vol. 17, pp. 573–587, 1997.

Kohei Hongo was born in Sendai, Japan in 1939. He received the B.E.E., M.E.E., and D.E.E. degrees, all from Tohoku University, Sendai, Japan, in 1962, 1964, and 1967, respectively.

From 1967 to 1968, he was an Assistant in the Faculty of Engineering, Tohoku University, Sendai. In 1968 he joined Shizuoka University, Hamamatsu, Japan, as a Lecturer. In 1969 he became an Assistant Professor and in 1979 promoted to Professor. From 1974 to 1975 he was Visiting Associate Professor at the University of Illinois, Urbana-Champaign, and in 1982, he visited Hei-Long-Jian University, Harbin, China, as a Guest Lecturer. In 1991 he became a freelance consultant and in 1992 he joined the Faculty of Science as a professor at Toho University, Hunabashi City, Chiba, Japan. His research interests include development of physical theory of diffraction with transition currents and application of Kobayashi potential (technique of analysing mixed boundary value problems) to more realistic diffraction problems.

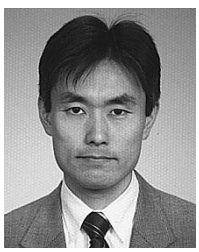

Hirohide Serizawa was born in Shizuoka Prefecture, Japan, on April 7, 1965. He received the B.E. and M.E. degrees from Shizuoka University, Hamamatsu, Japan, in 1988 and 1990, respectively.

From April 1990 to March 1998, he was an Associate Researcher at Numazu College of Technology (NCT), Numazu, Japan, and is currently an Assistant Professor there. From 1997 to 1998 he was with Toho University, Funabashi, Japan, as a Visiting Researcher on leave from NCT. His research interest is the application of Kobayashi potential (KP) method to diffraction problem.